Le, T; Striolo, A; Cole, D. CO_2–C_4H_{10} Mixtures Simulated in Silica Slit Pores: Relation between Structure and Dynamics. *J. Phys. Chem. C*, 2015, 119 (27), pp 15274–15284. DOI: 10.1021/acs.jpcc.5b03160

Article

CO_2-C_4H_{10} Mixtures Simulated in Silica Slit Pores: Relation between Structure and Dynamics

*Thu Le and Alberto Striolo**
Department of Chemical Engineering, University College London, London WC1E 6BT United Kingdom

David R. Cole
School of Earth Sciences, The Ohio State University, Columbus, Ohio 43210 United States

ABSTRACT

Equilibrium molecular dynamics simulations were conducted for pure n-butane and for mixtures containing n-butane and carbon dioxide confined in 2 nm wide slit-shaped pores carved out of cristobalite silica. A range of thermodynamic conditions was explored, including temperatures ranging from sub-critical to super-critical, and various densities. Preferential adsorption of carbon dioxide near the –OH groups on the surface was observed, where the adsorbed CO_2 molecules tend to interact simultaneously with more than one –OH group. Analysis of the simulation results suggests that the preferential CO_2 adsorption to the pore walls weakens the adsorption of n-butane, lowers the activation energy for n-butane diffusivity, and consequently enhances n-butane mobility. The diffusion results obtained for pure CO_2 are consistent with strong adsorption on the pore walls, as the CO_2 self-diffusion coefficient is low at low densities, increases with loading, and exhibits a maximum as the density is increased further because of hindrance effects. As the temperature increases, the maximum in self-diffusion coefficient is narrower, steeper and shifted to lower loading. The simulation results are also quantified in terms of molecular density profiles for both butane and CO_2 and in terms of residence time of the various molecules near the solid substrate. Our results could be useful for designing separation devices and also for better understanding the behavior of fluids in sub-surface environments.

* Author to whom correspondence should be addressed: a.striolo@ucl.ac.uk

Keywords: Competitive Adsorption; Diffusion

INTRODUCTION

International attention on curbing anthropogenic CO_2 emissions has recently increased dramatically.[1-3] Among other technologies, CO_2 capture and storage (CCS) is considered one of the most attractive alternatives.[4] Some pilot CCS projects have been initiated. In Sleipner (west Norway) 1 million metric tons of CO_2 have been injected annually, since 1996, into sedimentary basins.[5] Recently, CO_2 has also been injected into basaltic formations, because their high content of Ca, Mg, and Fe suggests the possibility of achieving CO_2 mineralization.[6-8] CO_2 sequestration combined with enhanced coal bed methane recovery has also been extensively studied,[9-10,11,12] and CO_2 injection is often used in tertiary enhanced oil recovery in depleted petroleum reservoirs.[13] Lately, CO_2 has also been used in fracturing fluids for shale gas stimulation.[14-15] Not only CO_2 can be captured and stored within the shale formation, recent results suggest that in some cases CO_2 can create better fractured networks compared to water.[16] Should CO_2 exhibit higher affinity to the rock formations than hydrocarbons, it could help increase production. Understanding the relation between competitive adsorption and transport of CO_2 and hydrocarbons in rock formations is considered crucial to optimize both CO_2 storage capacity[17] and natural gas production.

Much is known about structure and dynamics of carbon dioxide and methane confined in activated carbons,[18] carbon nanotubes (CNTs),[19] and zeolites.[20-22] The transport of CO_2 through silica has been studied using experiments[23-24] and simulations.[23, 25-26] Experimental and simulation results confirm the preferential adsorption of CO_2 from binary CO_2/CH_4 mixtures. High CO_2 adsorption selectivity was observed in CNTs.[19] An extensive review on CO_2 and methane storage in hybrid porous solids, crystallized porous materials including MOFs, and porous coordination polymers was compiled by Ferey et al.,[27] who summarized structural, spectroscopic, thermodynamics experiments as well as molecular simulation results. Because of the intrinsic limitations of experiments, thermodynamic models, and simulations, holistic approaches inclusive of all such contributions are needed to completely understand complex phenomena such as those just discussed. As opposed to the extensive literature on pure CO_2 and CH_4 and on their binary mixtures, few results are available for mixtures of CO_2 and higher molecular weight hydrocarbons such as butane and octane in microporous confinement.

We previously conducted extensive molecular dynamics (MD) simulations to study propane adsorption, structure and diffusion in slit-shaped silica pores at sub-, near-, and super-critical conditions.[28] The results were qualitatively consistent with the experimental adsorption isotherms reported by Gruszkiewicz et al.,[29] and the SANS data reported by Rother et al.[30] We recently conducted MD simulations for the structure and dynamics of CO_2-octane mixtures confined within slit-shaped silica pores (unpublished results). Building on these efforts, we present here structural (i.e., density profiles, molecular orientation, and preferential adsorption sites) and dynamic properties (i.e., self-diffusion coefficients and residence times at contact with the solid surface) for mixtures containing n-butane and CO_2 confined in slit-shaped silica pores. Silica is chosen because quartz can be an abundant sub-surface material. β-cristobalite was used to compare the new results to those our group has obtained for several fluids under confinement. We investigate the effect of mixture density and composition on adsorption and diffusion of the confined fluids. We consider temperatures below, between, and above the critical temperatures of CO_2 and n-butane. MD simulations are chosen in the present investigation for their ability to provide extensive insights regarding effective fluid-solids interactions, structural and dynamic properties of all components of interest.

SIMULATION MODELS AND METHODOLOGY

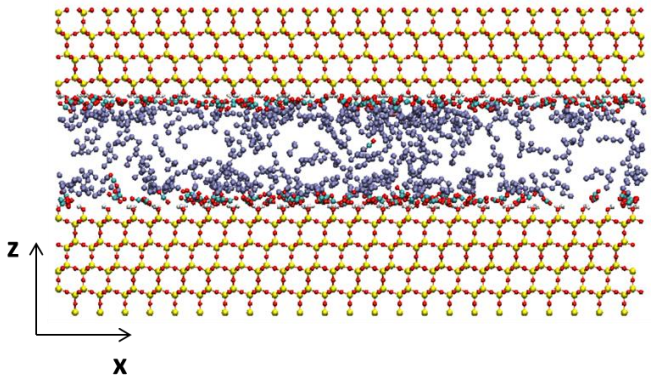

Figure 1. Simulation snapshot representing a simulation box containing 250 CO_2 and 250 n-C_4H_{10} molecules in the 2 nm silica pore at 343K. The solid silica slabs are continuous along both X and Y directions. No bulk region exists. Purple spheres are CH_2 and CH_3 groups in n-butane, cyan is C in carbon dioxide, red is O, white is H, and yellow is Si.

Extensive MD simulations for binary mixtures of CO_2/n-C_4H_{10} confined within slit-shaped silica pores were performed. The silica surfaces used in this work were obtained by cutting the β-cristobalite SiO_2 crystal along the (1 1 1) crystallographic face. A detailed description of the solid morphology was provided previously.[28, 31] Because quartz (made up of SiO_4 tetrahedra groups) is an abundant mineral in earth, the cristobalite crystal is considered here as a proxy for hydrophilic rock pore surfaces.[32] We are conducting simulation results on models for other minerals. The results, when available, will allow us to better quantify the effect of mineral properties on fluid behavior. The pore width is 2 nm and the corresponding simulation box dimensions are 10.48x10.08x5.34 nm^3. In pores as narrow as the one chosen for the present study interfacial interactions are expected to dictate the confined fluid behavior. Note that transport of fluid through pore throats of this width, and perhaps narrower, is expected to impact the permeability in shale rocks.[33] The effective pore volume in our model system was estimated in approximately 214.83 nm^3. Because of periodic boundary conditions, the systems considered are composed by silica slabs that are infinitely long along the X and Y directions, and separated along the Z direction by the slit-shaped pore. The solid substrate bears no net charge, and all the non-bridging O atoms in the solid are fully protonated, yielding a high density of surface –OH groups.

The experimental critical temperatures of CO_2 and C_4H_{10} are 304.13K and 425.125K, respectively.[34] To investigate the properties of the mixtures as the temperature changes from sub- to super-critical, 3 temperatures were chosen: 290K (below the critical *T* of both fluids), 343K and 430K (above the critical *T* of both fluids). Different densities of the confined mixtures (100, 300 and 500 total molecules) and different mixture compositions (CO_2:n-C_4H_{10}=1:9, 5:5 and 9:1) were considered. In **Figure 1** we represent the pore with 250 CO_2 and 250 n-butane molecules.

The total system energy is obtained as the sum of dispersive (van der Waals), electrostatic, bond stretch, bond angle, and dihedral interactions:

$$E_{total} = E_{VDW} + E_{\text{electrostatic}} + E_{bond\ stretch} + E_{angle\ bend} + E_{dihedral} \quad (1)$$

E_{VDW} and $E_{electrostatic}$ are expressed by 12-6 Lennard-Jones and Coulombic potentials, respectively. Lennard-Jones parameters for non-like components were obtained using Lorentz-Berthelot mixing rules from the values of the pure compounds.[35-37] Intramolecular potentials were represented by harmonic functions. The CLAYFF force field[38] was implemented to simulate the silica substrate while carbon dioxide and butane were modeled using the TraPPE-UA force field.[39] Simulations performed implementing the TraPPE force field yield the critical temperatures of 306.2[40] and 423.4K[39] for CO_2 and n-butane, respectively. Within our simulations CO_2 is rigid with all atoms on a straight line while butane is a flexible molecule described by bond stretching, angle bending, and dihedral constraints. Methyl (CH_3) and ethyl (CH_2) groups of n-butane are treated within the united-atom formalism. The hydrocarbon does not bear partial charges. All atoms on the solid silica, except for H of the surface –OH groups, remain rigid throughout the whole length of the simulations.

While the algorithms used to calculate the results reported here are described in our previous work,[41] it is worth discussing the methodology implemented to investigate the activation energy for diffusion. The diffusivity of the fluids within the pore is considered as a 2-dimensional translation along the X and Y directions, because the movement along the Z direction is constrained by the confining pore surfaces. To obtain the planar self-diffusion coefficient D_s we calculated the mean square displacement (MSD) following established procedures.[28] The fluid diffusion, which is dominated by steric effects and solid-fluid interactions,[42] can be described as an activated process using the Arrhenius formalism:

$$D(0) = D_f e^{\left(\frac{-E_a}{RT}\right)} \quad (2)$$

In this equation $D(0)$ is the self-diffusion coefficient at infinite dilution, D_f is the pre-factor, E_a the activation energy, R the gas constant, and T the absolute temperature. By plotting ln $D(0)$ as a function of $1/T$, we should obtain a straight line whose slope is $\frac{-E_a}{R}$.

To estimate the effect of CO_2 on the activation energy of butane diffusion, and in particular the role of electrostatic interactions between CO_2 and the solid substrate on E_a, we applied Eq. (2) to fit results obtained for n-butane (1) at infinite dilution in CO_2 (the system contained 500 CO_2 and 2 C_4H_{10} molecules); (2) at infinite dilution in a model fluid obtained by setting all partial charges of CO_2 to zero (while not changing the CO_2 Lennard-Jones parameters; i.e., pseudo-CO_2); and (3) at vanishing density (only 2 butane molecules with no other fluid present).

All simulations were carried out within orthorhombic simulation boxes containing a constant number of molecules at fixed volume and constant T. T of silica and fluid were controlled separately by two Nosé-Hoover thermostats[43-44] with relaxation times of 200 fs each. Corrections for long-range electrostatic interactions were taken into account by the particle-mesh Ewald summation.[45] The cutoff distance for all interactions was set at 14 Å. The simulations were conducted using the Groningen Machine for Chemical Simulations

(GROMACS) simulation package, version 4.5.5.[46-47] The leapfrog algorithm[48] with time steps of 1 fs was implemented. Simulations were conducted for 100 ns of simulation time for all systems investigated. Equilibration was considered achieved after ~50-80 ns, depending on the system loading, when the system temperature, total energy and density profiles fluctuate around constant values (+/- 15%). Data analysis was carried out over the last 10 ns of each simulation. All results were calculated considering the center of mass (COM) of the fluid molecules.

RESULTS AND DISCUSSIONS

Structural Properties

Molecular Density Profiles

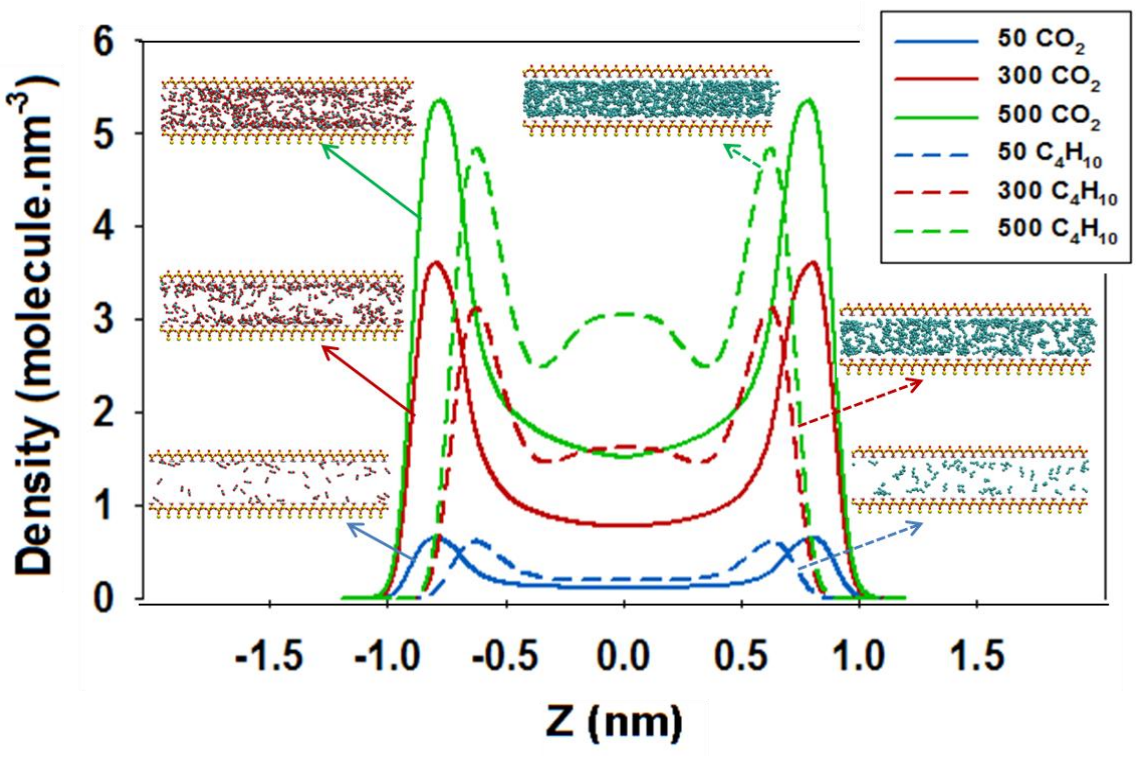

Figure 2. Molecular density profiles for carbon dioxide (solid lines) and n-butane (dashed lines) with corresponding simulation snapshot for pure component systems with 50, 300 and 500 molecules at 430K. Z is the direction perpendicular to the pore surface and Z=0 corresponds to the pore center. The color code is the same as that used in **Figure 1**. Only 2 inner atomic layers of the pore surfaces are shown for clarity. Note that the results presented in this figure are for single-component systems.

Molecular density profiles along the direction perpendicular to the pore surface were calculated for all simulated systems. Representative density profiles for single-component systems of both species at increasing loadings (50, 300 and 500 molecules within the simulated system) at 430K are presented in **Figure 2**. The results show that CO_2 adsorbs more closely to the pore walls even at this relatively high temperature compared to butane, presumably because of preferential interactions with the surface groups, and perhaps because of the flexibility of n-butane (note that the density profiles are obtained for the COM of n-butane), which contributes to maintaining this molecule slightly farther from the surface because of entropic effects. Simulation snapshots for the corresponding systems are provided in **Figure 2** for visualization purposes.

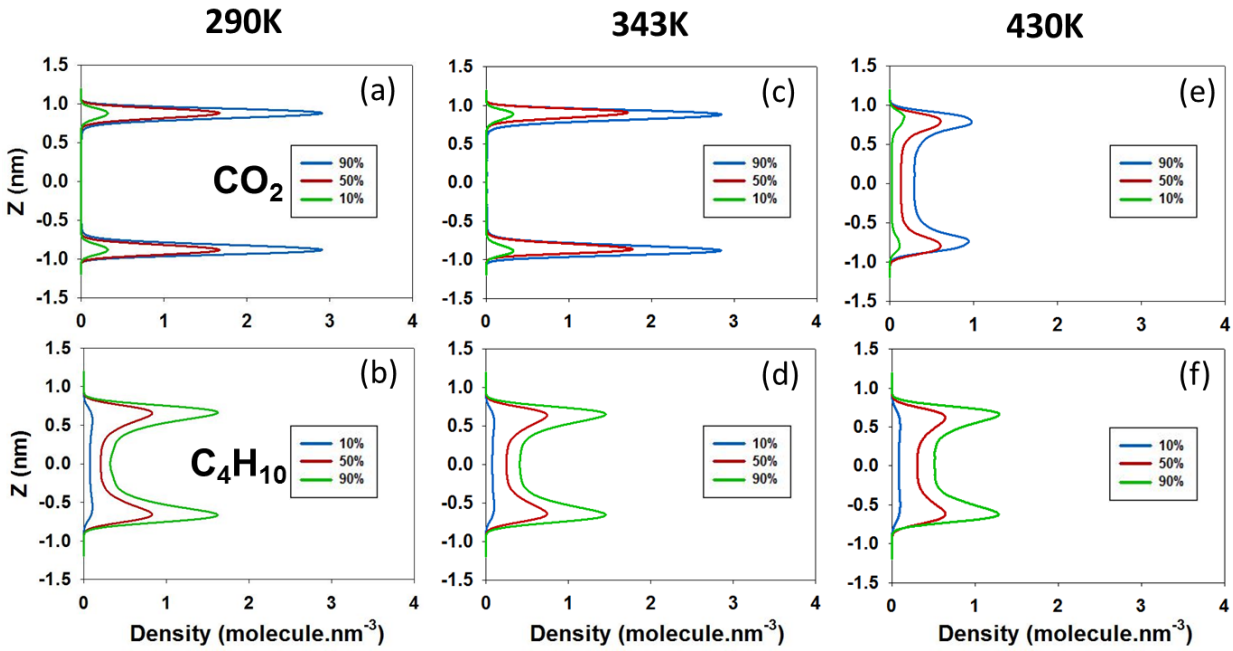

Figure 3. Molecular density profiles for carbon dioxide (top panels) and n-butane (bottom panels) in mixture containing a total of 100 molecules at 290, 343, and 430K. Z is the direction perpendicular to the pore surface and Z=0 corresponds to the pore center. Different lines represent results at different compositions. Blue, red and green lines represent mixtures with CO_2:n-C_4H_{10} molecular ratios of 9:1, 5:5 and 1:9, respectively.

Results obtained at different temperatures and mixture compositions are shown in **Figure 3, 4** and **5**, where CO_2 (top panels) and n-C_4H_{10} (bottom panels) profiles are computed separately. **Figures 3, 4,** and **5** are for systems with a total of 100, 300 and 500 fluid molecules, respectively, at different CO_2 vs. n-C_4H_{10} composition.

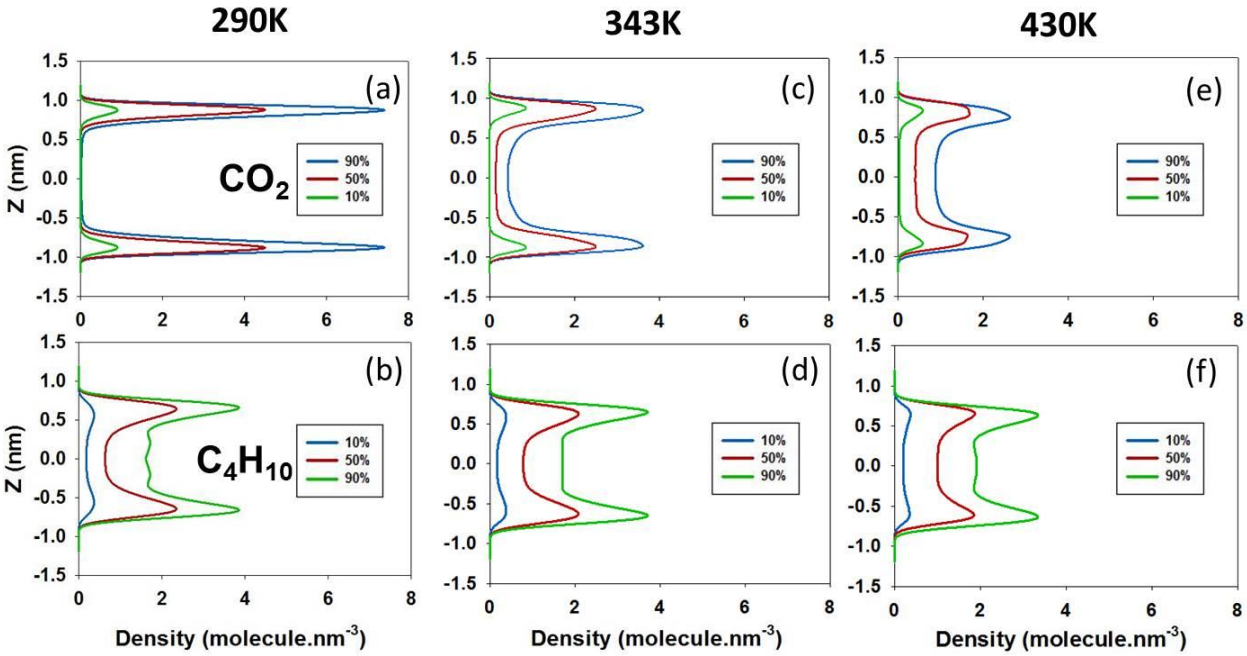

Figure 4. Same as **Figure 3** for mixture containing a total of 300 molecules.

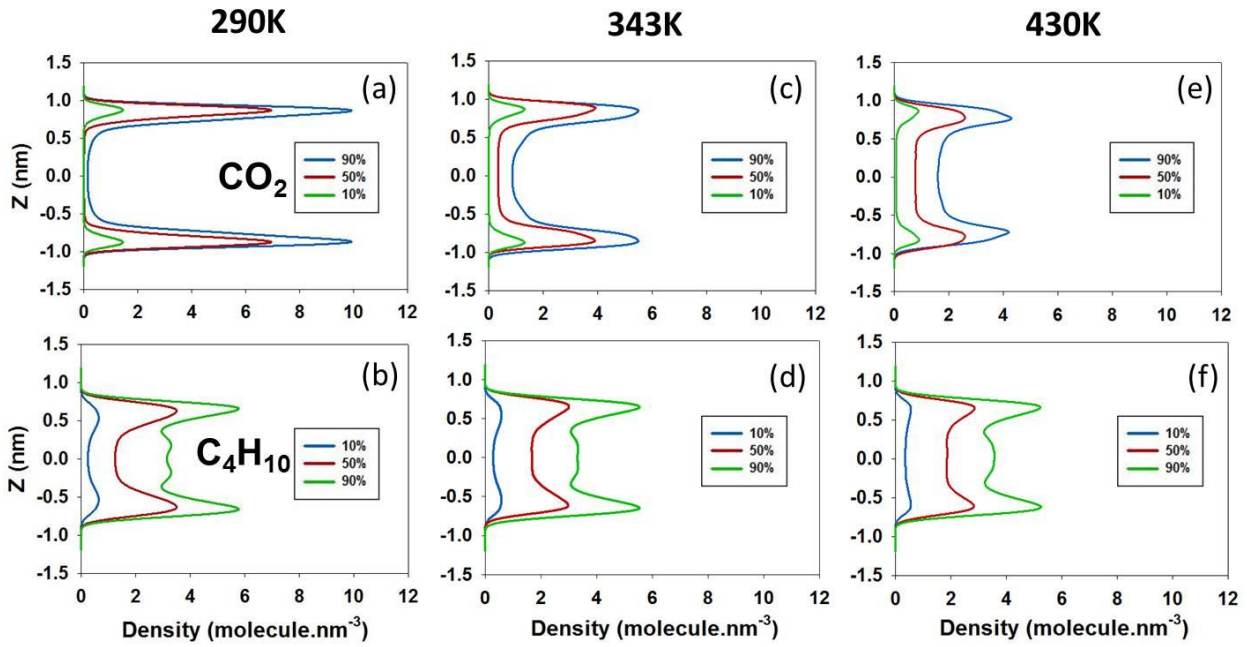

Figure 5. Same as **Figure 3** for mixture containing a total of 500 molecules.

The results in each pair of *vertical* panels in **Figure 3, 4** and **5** were obtained at constant temperature and density, but different composition. The molecular ratios CO_2:n-C_4H_{10} investigated were 9:1, 5:5 and 1:9 (blue, red and green lines, respectively). The molecular density profiles are shown as a function of the distance from the pore center (Z=0). For each curve, there are two distinct peaks (symmetric with respect to the pore center) that are localized near the pore surface. These are due to the adsorption of either CO_2 or butane on the pore walls. At high densities (i.e., 500 molecules) multiple peaks are observed in the density profiles obtained for butane, especially when the mixture composition is 90% C_4H_{10}, at the lowest temperature considered, suggesting the formation of a multi-layered structure. On the contrary, no CO_2 multilayer was observed at any condition considered. The results also show that the location of CO_2 peaks does not depend on *T*, and that this location is always close to the pore surfaces. The fact that the CO_2 density peaks are always closer to the pore walls than the butane density peaks indicates preferential CO_2 adsorption on the protonated silica surfaces, presumably because of the polar interactions between CO_2 and the surface –OH groups. The CO_2 peaks are higher and narrower at lower *T*, because of reduced thermal motion.[49] Note that while at low CO_2 concentration no CO_2 is found, statistically, near the pore center, butane molecules are always found near the pore center even at the lower butane concentrations considered here, suggesting that CO_2-pore attractions are stronger than butane-pore ones. As *T* and concentration rise, CO_2 can also be found near the pore center. The strong association between CO_2 and the pore surface revealed by our simulations is qualitatively consistent with recent experimental results reported by Rother et al. for CO_2 in porous silica aerogels.[50] The results discussed so far are qualitatively consistent with those we recently obtained for CO_2-octane systems confined in a silica pore similar to the one considered here, in which case it was found that adding small amounts of CO_2 could displace the location of the octane density peaks further away from the surface compared to the results obtained for the pure hydrocarbon (unpublished results).

Planar Density Distributions: Localization of Preferential Adsorption Sites

To document the molecular structure of the adsorbed CO_2 layer and to identify the preferential adsorption sites on the silica substrates we calculated in-plane density distributions. The calculations were performed for the oxygen atoms of those CO_2 molecules found within the first adsorption layers (see **Figure 3-5**) parallel to the pore surface and of 5 Å in thickness. Similar calculations were performed for the COM of those n-butane molecules found within the first adsorption layer of thickness 3.8 Å as identified by the density profiles shown in **Figure 3-5**. These types of calculations provide greater detail on the structure of the first hydration layer and/or of the first solvation layer on various substrates.[31, 51] In **Figure 6,** panels (b) and (c), respectively, we present the results obtained in this work. Both data sets are obtained for systems in which either CO_2 (panel b) or butane (panel c) are the main component within the fluid system. The results show that it is highly probable to find the oxygen atoms of adsorbed CO_2 molecules near the surface –OH groups of the solid silica substrate. This is expected, as CO_2 molecules can form hydrogen bonds with the –OH groups. According to the IUPAC definition, a hydrogen bond is "an attractive interaction between a hydrogen atom from a molecule or a molecular fragment X–H in which X is more electronegative than H, and an atom or a group of atoms in the same or a different molecule, in which there is evidence of bond formation".[52] Sato et al. provided evidence for a hydrogen bond between CO_2 and water,[53] suggesting that hydrogen bonds between CO_2 and surface –OH groups are possible. The results obtained for butane show that these molecules accumulate along the hexagonal edges of the atomic structure of the solid substrate, suggesting that non-specific dispersive interactions

are responsible for the formation of the first adsorbed layer of butane near the flat solid surface reported in the density profiles discussed in **Figures 2-5** above. The planar density profiles for butane in **Figure 6** are a little smeared because we are considering the COM of the molecule rather than the individual atoms.

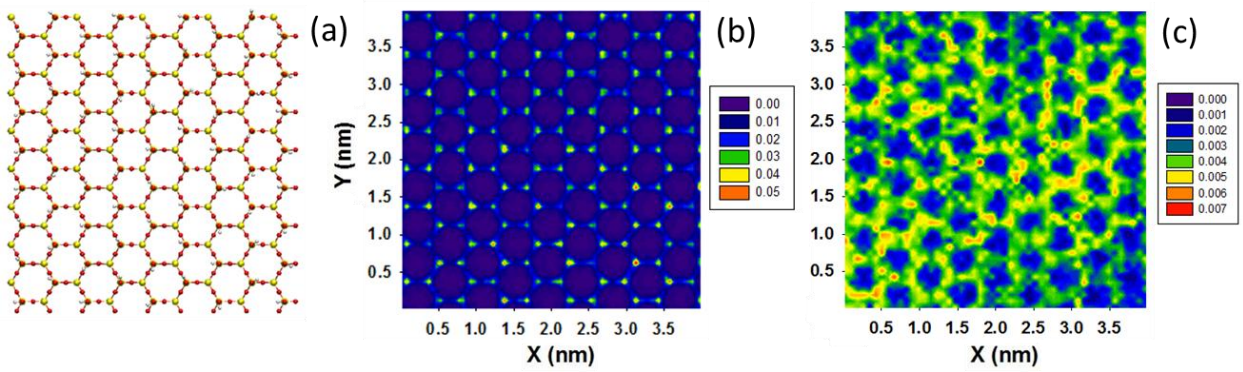

Figure 6. (a) OH-terminated silica surfaces. Only the upper 2 atomic layers are shown for clarity. (b) Planar density distribution of O atoms of CO_2 molecules within the first adsorption layer when 500 molecules, 90% CO_2, are simulated at 290K. (c) Planar density distribution of the COM of n-butane within the first adsorption layer for a system composed of 500 molecules (90% butane) at 290K. Densities are expressed in number of atoms/molecules.nm^{-3}. Note that the densities in panels (b) and (c) are of different orders of magnitude.

Orientation of Adsorbed CO_2

In **Figure 7**, we report the preferential orientation of adsorbed carbon dioxide molecules. The molecules considered are those within the first adsorbed layer, as discussed in the prior section. We quantified the probability distribution of the angle θ formed between the CO_2 backbone and the surface normal. When θ is 0° or 180°, the CO_2 molecule is perpendicular to the surface; when θ is 90°, CO_2 lays parallel to the surface. See **Figure 7** panel (a) for an illustration. The results obtained for the system comprised of 150 CO_2 and 150 n-butane molecules at 343K is shown in panel (b). The results show that CO_2 molecules within the first adsorbed layer preferentially orient at an angle θ of ~80°. While the preferential orientation angle of ~80° with the surface normal is observed in all systems considered, the local minimum in the orientation observed at ~90° is less pronounced when the simulation temperature decreases, and when the CO_2 loading decreases. As the substrate –OH and CO_2 molecules can form hydrogen bonds, the most energetically favorable configuration is expected to be the one where –OH and O–C–O lay on a straight line. Because the silanol Si–O–H group has an angle of ~109.5°, θ was thought to be ~70.5°. The fact that θ is ~9.5° larger indicates that each adsorbed CO_2 molecule tends to interact simultaneously with more than one surface –OH at a time. This becomes slightly more pronounced when *T* and CO_2 loading are lowered. This result is consistent with prior results obtained from the simulation of n-octane – CO_2 mixtures confined in silica pores (unpublished results). In that contribution we investigated systems at increasing CO_2 loadings and we concluded that, on average, when the amount of CO_2 present is sufficient to saturate the pore surface considered, one CO_2 molecule occupies two surface –OH groups.

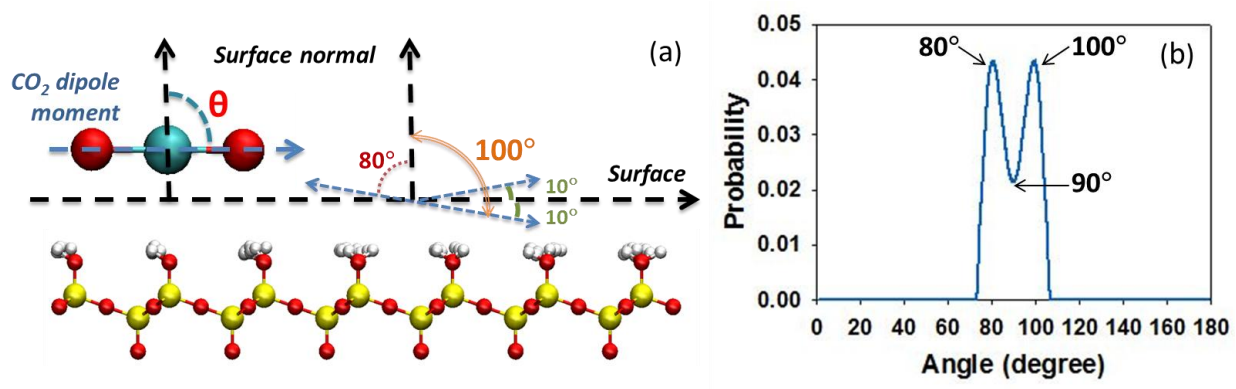

Figure 7. (a) Schematic for the orientation of one adsorbed carbon dioxide molecule. The color scheme for the solid substrate and CO_2 model is the same as that of **Figure 1**; (b) Probability density distribution for the angle θ for CO_2 molecules adsorbed within the first layer adsorbed of 5 Å thickness in silica pore. The results are obtained for the system composed of 150 CO_2 and 150 n-butane at 343K.

Dynamical Properties

Diffusivity – Pure substances

Single-component self-diffusion coefficients of (1) CO_2 at 290, 343 and 430K and (2) n-butane at 430K are calculated and presented in **Figure 8**. Results obtained for pure CO_2 at different temperatures show a maximum in D_s as loading increases from a near-zero loading. The maximum is narrower, steeper and shifted to lower loadings as T increases. CO_2 self-diffusion results match the type IV behavior as classified by Karger and Pfeifer.[54] CO_2 diffusion results are in good qualitative agreement with those reported by Sholl,[55] who represented an adsorbent using a lattice with heterogeneous adsorption sites and fluid species characterized by different adsorption energies (i.e., very strong attractive sites for specie 1 and no energetic preferences for specie 2). Our results are consistent with those obtained for the fluid specie that is strongly adsorbed on preferential sites available on the lattice: at low loadings, most particles of this fluid are trapped near the correspondent adsorption sites, and diffusion is dominated by slow hopping events between strong adsorption sites. At moderate loadings, those molecules that are not trapped can diffuse rapidly and the overall diffusivity increases. At high loadings, the diffusion coefficient decreases because of steric hindrance. Our results show that at 430K the self-diffusion coefficient of pure CO_2 displays a maximum at intermediate loadings while that of pure C_4H_{10} monotonically decreases with increasing loading (panel b). The results for butane are also consistent with those presented by Sholl,[55] when the fluid is not strongly attracted to lattice sites, in which case the self-diffusion coefficient monotonically decreases as loading increases. At 430K, D_s of CO_2 is higher than that of C_4H_{10} except at very low loadings. Visualizations of sequences of simulation snapshots suggest that CO_2 diffusion occurs predominantly along the surface, while butane moves across the pore volume, which is in agreement with the density profiles shown above. It is possible that the self-diffusion coefficient of CO_2 is faster than that of butane because the former molecule is smaller and slender than the latter. Babarao and Jiang investigated CO_2 and CH_4 transport across nano-porous materials

with pore sizes in the range of ~7 – 9 Å; their results show that steric hindrance causes a decrease in self-diffusion coefficient as loading increases for both substances.[42]

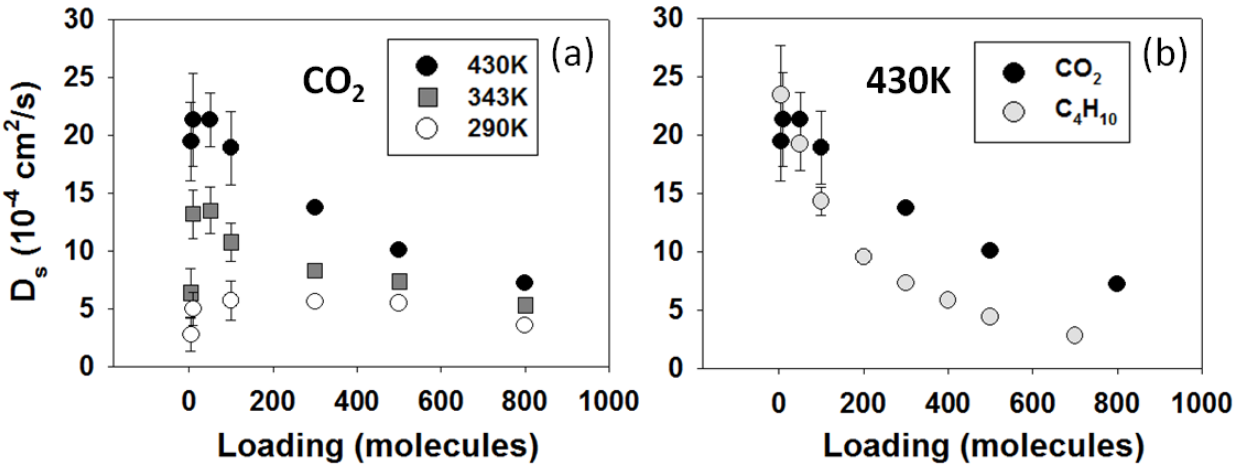

Figure 8. Single-component self-diffusion coefficients as a function of loading for (a) CO_2 at different temperatures and (b) CO_2 and C_4H_{10} at 430K. Note that these results are obtained for pure n-butane and CO_2, not their mixtures. Error bars are estimated as one standard deviation from the average. At high loadings, symbols are larger than error bars.

Diffusivity – Mixtures

Calculated CO_2 and n-C_4H_{10} two-dimensional self-diffusion coefficients at different mixture densities and compositions are presented in **Tables 1** and **2**. In general, the mobility of both fluids increases with increasing *T* and decreasing mixture density (lower total number of molecules) because higher *T* increases the kinetic energy of the molecules, while lower density reduces molecular collisions and steric hindrance. When binary mixtures are considered, our results show that D_s for CO_2 increases as its concentration increases, at a given total pore loading, with maximum D_s observed for 100% CO_2. A similar observation was reported by Wang et al.[56] in their experimental study for the diffusion of various alkanes in microporous BPL activated carbon. These results are explained as follows: at low loadings, adsorbate molecules are strongly adsorbed on high-energy adsorption sites, which results in low diffusion coefficients. As the amount adsorbed increases, the high-energy adsorption sites are saturated, and the diffusion statistically increases because adsorbate molecules have more mobility. Note that while CO_2 is preferentially adsorbed on the surface –OH groups in our model adsorbent, alkanes are strongly adsorbed on activated carbons. Observations similar to those reported herein were obtained also for systems comprising of n-octane and CO_2 (unpublished results), but not for systems comprised of only propane, because in the latter case no high-energy adsorption sites are available for propane on the fully protonated silica surfaces.[28] The increased mobility of CO_2 upon increasing its concentration at constant pore loading is consistent with results reported by Snurr and Karger[57] for methane and tetraflouromethane mixtures in silicalite. By performing both MD simulations and NMR experiments, at the total loading for 12 molecules per unit cell, the diffusivities of both fluids were found to increase with

increasing amount of CH_4, which is the lighter and more mobile component. At constant loading (number of molecules), our results show that the self-diffusion coefficient for butane decreases as the amount of CO_2 decreases. This could be due to steric hindrance (butane is larger than CO_2), and to changes in the activation energy of butane diffusion due to CO_2 (discussed below). The decrease of the activation energy due to CO_2, is consistent with observations reported by Vidoni.[58] This latter study experimentally measured the competitive diffusion of CH_4 with either He or CO_2 in DD3R crystals using the zero length column method. The results showed reduced activation energy for diffusion of CH_4-CO_2 compared to CH_4-He due to the competitive adsorption of carbon dioxide on the pore surfaces.

Table 1. In-plane self-diffusion coefficients estimated for CO_2

	CO_2 Calculated Diffusion Coefficient (10^{-4} cm^2/s)			
Total number of molecules	Composition (CO_2:C_4H_{10})	290K	343K	430K
100	Pure CO_2	*5.7 ± 1.1*	*10.8 ± 1.6*	*18.9 ± 3.4*
	9:1	3.5 ± 0.8	8.5 ± 1.3	15.1 ± 1.9
	5:5	1.5 ± 0.3	3.7 ± 1.8	12.2 ± 2.8
	1:9	1.1 ± 0.2	2.5 ± 1.4	6.6 ± 1.2
	Bulk CO_2	42.7 ± 5.6 (vapor, 1.68 MPa)	57.0 ± 6.2 (vapor, 2.06 MPa)	64.8 ± 7.5 (vapor, 2.7 MPa)
300	Pure CO_2	*5.6 ± 2.2*	*8.3 ± 0.2*	*13.7 ± 0.1*
	9:1	3.5 ± 0.3	5.8 ± 0.4	11.6 ± 0.4
	5:5	1.3 ± 0.1	2.8 ± 0.4	7.4 ± 1.0
	1:9	1.2 ± 0.2	2.7 ± 0.2	4.8 ± 1.7
	Bulk CO_2	16.0 ± 3.7 (vapor, 4.04 MPa)	18.6 ± 4.7 (vapor, 5.39 MPa)	21.8 ± 1.6 (s.c.,[1] 7.46 MPa)
500	Pure CO_2	*5.5 ± 1.5*	*7.4 ± 0.3*	*10.1 ± 0.3*
	9:1	3.3 ± 0.3	5.0 ± 0.4	8.7 ± 1.0
	5:5	1.4 ± 0.1	2.5 ± 0.4	5.5 ± 2.0
	1:9	0.7 ± 0.1	2.0 ± 0.1	4.1 ± 1.0
	Bulk CO_2	9.1 ± 0.7 (vapor, 5.30 MPa)	9.8 ± 1.6 (s.c.,[1] 7.88 MPa)	12.6 ± 1.0 (s.c.,[1] 11.74 MPa)

[1]super critical

Table 2. In-plane self-diffusion coefficients estimated for C_4H_{10}

C_4H_{10} Calculated Diffusion Coefficient (10^{-4} cm^2/s)				
Total number of molecules	Composition (CO_2:C_4H_{10})	290K	343K	430K
100	9:1	12.9 ± 1.5	20.8 ± 4.3	22.3 ± 0.7
	5:5	9.4 ± 1.4	15.8 ± 2.1	18.2 ± 1.8
	1:9	7.9 ± 0.5	10.4 ± 1.1	13.5 ± 1.1
	Pure butane	*6.9 ± 0.6*	*9.8 ± 0.7*	*14.3 ± 1.2*
	Bulk butane	13.6 ± 0.4 (vapor) 0.8 ± 0.2 (liquid) (VLE,[1] 0.19 MPa)	14.8 ± 0.8 (vapor) 1.2 ± 0.2 (liquid) (VLE,[1] 0.8 MPa)	26.4 ± 6.0 (vapor, 2.16 MPa)
300	9:1	10.0 ± 0.5	14.5 ± 1.5	14.9 ± 0.6
	5:5	5.9 ± 1.1	8.4 ± 0.5	9.4 ± 1.0
	1:9	4.0 ± 0.3	6.0 ± 1.3	8.1 ± 1.0
	Pure butane	*3.5 ± 0.2*	*5.3 ± 0.2*	*7.3 ± 0.2*
	Bulk butane	13.6 ± 0.4 (vapor) 0.8 ± 0.2 (liquid) (VLE,[1] 0.19 MPa)	14.8 ± 0.8 (vapor) 1.2 ± 0.2 (liquid) (VLE,[1] 0.8 MPa)	7.6 ± 0.6 (s.c.,[2] 3.84 MPa)
500	9:1	6.4 ± 0.4	8.5 ± 0.4	8.6 ± 0.8
	5:5	3.9 ± 0.3	5.2 ± 0.4	7.2 ± 0.5
	1:9	2.5 ± 0.1	3.2 ± 0.1	4.7 ± 0.1
	Pure butane	*2.3 ± 0.1*	*3.5 ± 0.1*	*4.4 ± 0.1*
	Bulk butane	13.6 ± 0.4 (vapor) 0.8 ± 0.2 (liquid) (VLE,[1] 0.19 MPa)	14.8 ± 0.8 (vapor) 1.2 ± 0.2 (liquid) (VLE,[1] 0.8 MPa)	4.9 ± 0.3 (s.c.,[2] 4.1 MPa)

[1] vapor-liquid equilibrium
[2] super critical

For comparison, representative bulk properties of the pure substances are also provided in **Table 1** and **2**. The properties reported include the self-diffusion coefficient in three dimensions, and the physical state of the fluid at T and ρ conditions considered for the simulations of the confined fluids. The equilibrium states (vapor, liquid, vapor-liquid equilibrium or super-critical) for the bulk fluids and their pressures were extracted from the NIST database.[34] The self-diffusion coefficients were computed via bulk NVT simulations for 5 ns. The simulation results show that bulk self-diffusion coefficients for the pure fluids increase as T increases and decrease as ρ increases, as expected. All simulated values are in good agreement with literature data from both simulations and experiments.[59-61]

To assess the activation energy for C_4H_{10} diffusion in the pores considered here, in **Figure 9** we report the natural logarithm of C_4H_{10} self-diffusion coefficients at infinite dilution, $lnD(0)$, as a

function of the inverse temperature (T=290, 343, 430, 500 and 700 K). By fitting Eq. (2) to the data we extract E_a. The results shown in **Figure 9** are for three systems: two mixtures, each consisting of 2 butane and either 500 CO_2 or 500 pseudo CO_2 molecules, and pure butane at very low loading (empty circles). The simulations for butane at infinite dilution in the two mixtures are conducted to quantify the effect of electrostatic pore-CO_2 interactions on the butane diffusion. The pseudo CO_2 molecules bear no partial charges, although they are described by the Lennard-Jones parameters used to simulate CO_2 molecules. No preferential adsorption of pseudo CO_2 molecules to the solid substrates will occur, while steric effects will be similar for both mixtures. While the self-diffusion coefficients estimated for pure butane are the highest at high temperatures, we note that the calculated E_a for the pure butane at low loadings is 6.5±0.5 kJ/mol, while the activation energies for butane at infinite dilution in CO_2 and in the pseudo CO_2 systems are 3.4±0.9 and 5.7±0.9 kJ/mol, respectively. These results confirm that the electrostatic interactions between CO_2 and the pore surfaces, which cause preferential adsorption due to hydrogen bonds, is responsible for the enhanced hydrocarbon mobility observed in our simulations. While the pseudo CO_2 molecules also lower the activation energy compared to the system of pure butane at low loadings, pore crowding increases steric hindrance. The activation energies we report are consistent, albeit in the low range, with activation energies reported for the diffusion of fluids in other porous materials.[42, 58] Following literature observations, the fluid diffusion in our system is considered activated in light of the narrow pore size.[42, 62]

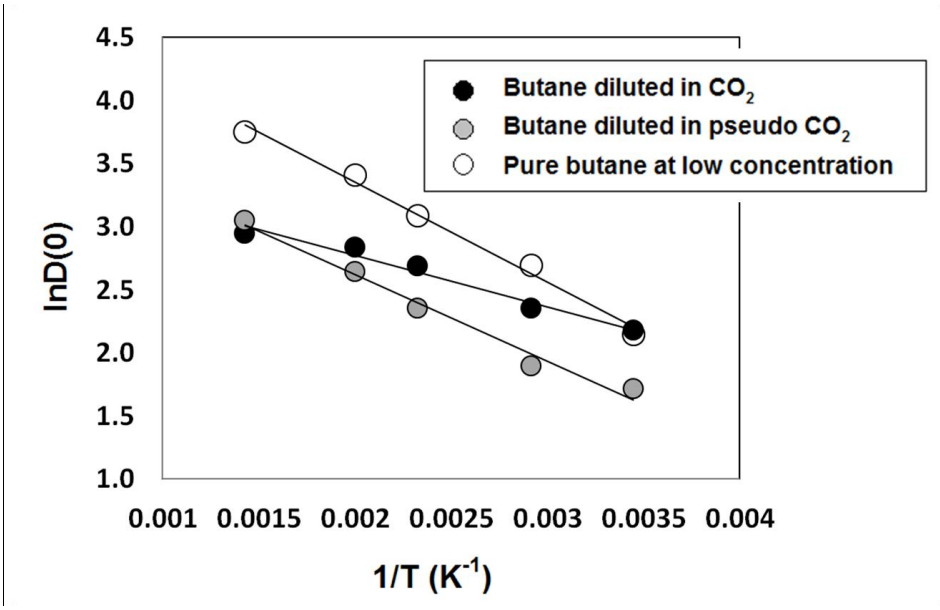

Figure 9. Arrhenius plot for the self-diffusion coefficient of n-C_4H_{10} confined in the silica pore at low concentration (empty circles), at infinite dilution in CO_2 molecules (black circles), and at infinite dilution in pseudo CO_2 molecules (gray circles). Symbols are calculated from simulations. Lines are the Arrhenius fits to the simulation data.

Residence Time near Pore Surfaces

We computed residence autocorrelation functions, $C_R(t)$, to quantify how long CO_2 and butane molecules remain in contact with the silica surfaces. The algorithm is described elsewhere.[63] We considered the COM of both CO_2 and butane to identify the position of one molecule. Only those molecules within the first adsorbed layers were considered. The faster C_R decays from 1 to 0, the faster the molecules leave the adsorbed layer. In **Figure 10** panel (a) we report the results obtained for CO_2 at different CO_2:C_4H_{10} molar ratios when a total of 100 molecules was present within the pore and T=290K. The results show that at the higher mole fraction of CO_2, the shorter it remains in the adsorbed layer, possibly due to faster exchanges between the adsorbed molecules and those near the pore center. At the lowest temperature and lowest concentration of CO_2 investigated (290K, 10 CO_2 molecules), $C_R(t)$ plateaus after 300 ps, suggesting that some of the adsorbed CO_2 molecules do not desorb within the simulation timeframe. The corresponding results obtained for butane are shown in **Figure 10** panel (b). In this case all the curves overlap for all mixture compositions, suggesting that butane molecules exchange between adsorbed and not-adsorbed states with the same frequency, irrespective of the amount of CO_2 present. This is probably due to the lack of strong attractions between butane and the pore surface. These results suggest that the decrease in activation energy for the n-butane diffusion is not related to the residence time of butane near the adsorbing surface. To support this observation it is worth pointing out that the density profiles obtained for n-butane in the direction perpendicular to the pore surface (**Figures 2-6**) always show peaks at the same distances from the surface, irrespectively on the amount of CO_2 present within the system.

In **Figure 11**, we report the residence autocorrelation functions of CO_2 molecules as a function of the total loading (top panels) and temperature (bottom panels) for *equimolar* binary mixtures. Because high temperature favors thermal motion and increased occurrence of fluid collisions that push the adsorbed molecules away from the interface, the residence autocorrelation function decreases faster with increasing temperature and/or density. At 430K, above the critical temperatures for both substances in the mixture, $C_R(t)$ curves overlap for all mixture compositions. The overlapping $C_R(t)$ results at 290K and 343K in panel (a) in **Figure 11** and the similarity of CO_2 density profiles in panel (a) and (c) of **Figure 3** suggest that at relatively low temperature and low fluids density, T and concentration have negligible effects on the adsorption of CO_2 on the pore wall, conditions at which pore-fluid interactions play the dominant role.

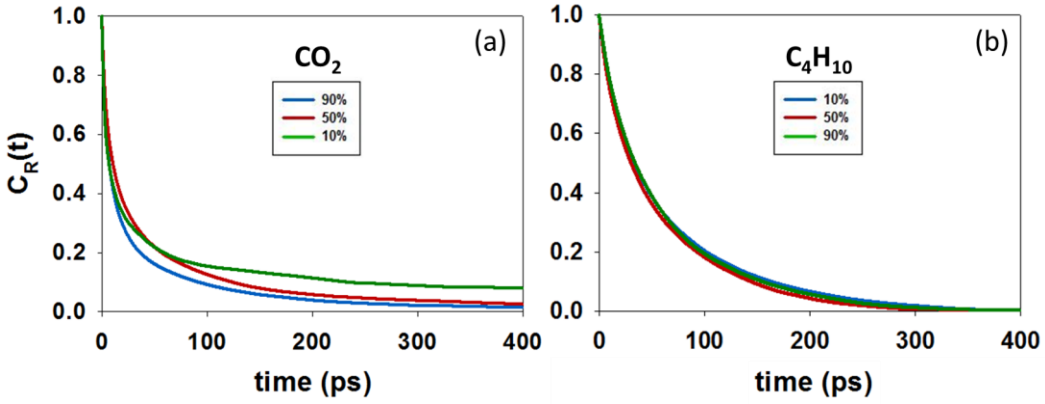

Figure 10. Representative residence autocorrelation functions, $C_R(t)$, for (a) CO_2 and (b) n-butane within the first adsorbed layers on the silica pore as a function of CO_2:C_4H_{10} molar ratio. Results are shown for the simulations conducted at 290K with 100 total molecules.

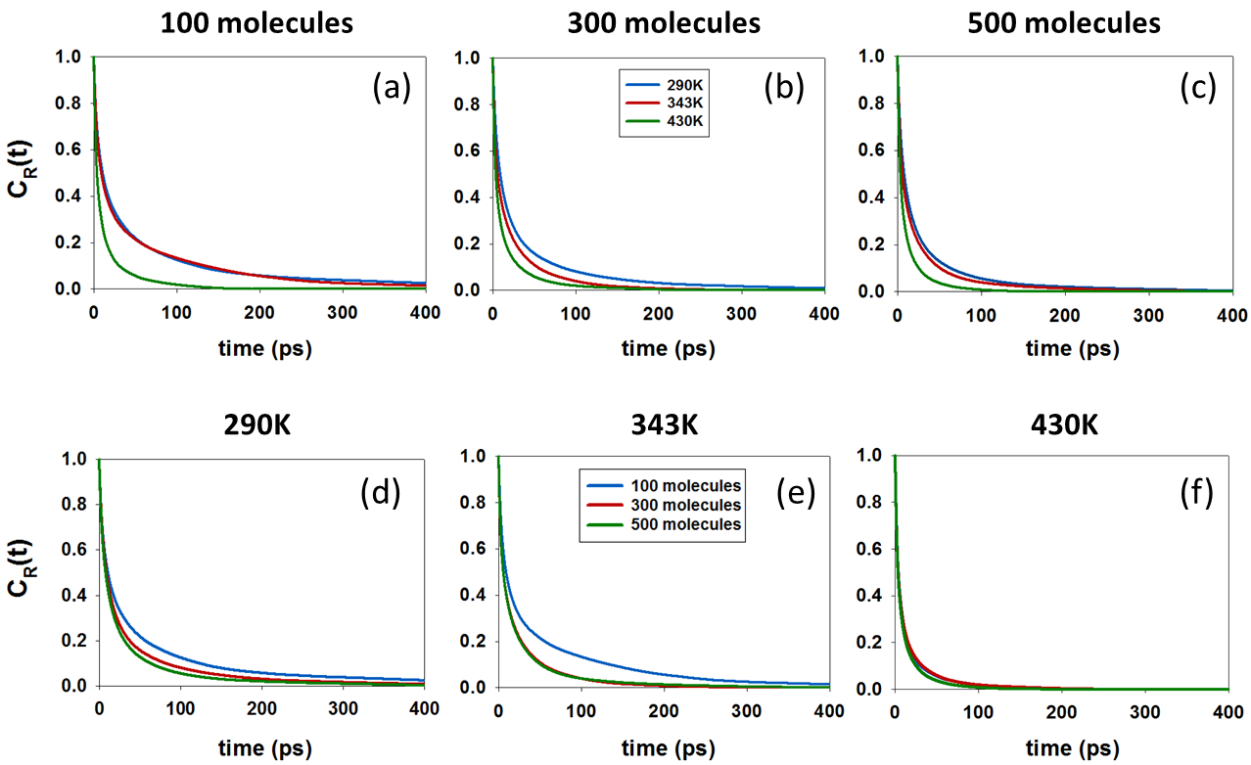

Figure 11. Residence autocorrelation functions, $C_R(t)$, for CO_2 within the first adsorbed layer as a function of the total number of molecules in mixture (top panels) and of temperature (bottom panels). In all cases the CO_2:C_4H_{10} molar ratio is 1:1.

CONCLUSIONS

Detailed molecular dynamics simulations were performed for systems consisting of pure carbon dioxide, pure n-butane, and their mixtures confined in fully protonated slit-shaped silica nanopores of width 2 nm. A range of temperatures (from sub- to super-critical), mixture densities and component ratios was considered. Our results show that CO_2 tends to interact with more than one –OH group on the substrate and that it preferentially adsorbs on the pore surface. CO_2 self-diffusion coefficients depend on pore loadings following the type IV behavior in the classification proposed by Karger and Pfeifer.[54] This is a consequence of the existence of high-energy adsorption sites (the surface –OH groups) that can strongly attract the CO_2. The self-diffusion coefficient of pure butane decreases as loading increases as a result of steric hindrance (type I behavior in the classification of Karger and Pfeifer). When mixtures are considered, at the same temperature and total molecular loading, carbon dioxide enhances the self-diffusion coefficient of n-butane by decreasing its diffusion activation energy. The results are corroborated by analysis of the average residence time of the various molecules at contact with the pore surfaces, density profiles in the direction perpendicular to the solid substrate, and parallel to the solid surface. Our results can be useful for designing separation devices, and perhaps planning CO_2 capture and storage strategies while optimizing natural gas production.

ACKNOWLEDGEMENTS

We acknowledge the financial support from the U.S. Department of Energy, Office of Basic Energy Sciences, under Contract No. DE-SC0006901 (Division of Chemical Sciences, Geosciences, and Biosciences). D.R.C. was supported under contract DE-SC0006878 provided by the U.S. Department of Energy, Office of Basic Energy Sciences (Division of Chemical Sciences, Geosciences, and Biosciences). Additional financial support was provided by the Sloan Foundation via the Deep Carbon Observatory. AS acknowledges financial support from the European Union via a Marie Curie Career Integration Grant. Generous allocations of computing time were provided by the Oklahoma Supercomputing Center for Education and Research (OSCER), Norman, OK, and by the National Energy Research Scientific Computing Center (NERSC) at Lawrence Berkeley National Laboratory, Berkeley, CA. NERSC is supported by the DOE Office of Science under Contract No. DE-AC02-05CH11231.

References

(1) Cox, P. M.; Betts, R. A.; Jones, C. D.; Spall, S. A.; Totterdell, I. J. Acceleration of Global Warming Due to Carbon-Cycle Feedbacks in a Coupled Climate Model. *Nature* **2000**, *408*, 184-187.

(2) Jenkinson, D. S.; Adams, D. E.; Wild, A. Model Estimates of CO_2 Emissions from Soil in Response to Global Warming. *Nature* **1991**, *351*, 304-306.

(3) Thomas, C. D.; Cameron, A.; Green, R. E.; Bakkenes, M.; Beaumont, L. J.; Collingham, Y. C.; Erasmus, B. F. N.; de Siqueira, M. F.; Grainger, A.; Hannah, L., et al. Extinction Risk from Climate Change. *Nature* **2004**, *427*, 145-148.

(4) Gaus, I. Role and Impact of CO_2–Rock Interactions During CO_2 Storage in Sedimentary Rocks. *Bull. Pol. Acad. Sci., Tech. Sci.* **2010**, *4*, 73-89.

(5) Gislason, S. R.; Oelkers, E. H. Carbon Storage in Basalt. *Science* **2014**, *344*, 373-374.

(6) Rosenbauer, R. J.; Thomas, B.; Bischoff, J. L.; Palandri, J. Carbon Sequestration Via Reaction with Basaltic Rocks: Geochemical Modeling and Experimental Results. *Geochim. Cosmochim. Ac.* **2012**, *89*, 116-133.

(7) Gislason, S. R.; Wolff-Boenisch, D.; Stefansson, A.; Oelkers, E. H.; Gunnlaugsson, E.; Sigurdardottir, H.; Sigfusson, B.; Broecker, W. S.; Matter, J. M.; Stute, M., et al. Mineral Sequestration of Carbon Dioxide in Basalt: A Pre-Injection Overview of the Carbfix Project. *Int. J. Greenh. Gas Control* **2010**, *4*, 537-545.

(8) Schaef, H. T.; McGrail, B. P.; Owen, A. T. Carbonate Mineralization of Volcanic Province Basalts. *Int. J. Greenh. Gas Control* **2010**, *4*, 249-261.

(9) Fathi, E.; Akkutlu, I. Y. In *Counter Diffusion and Competitive Adsorption Effects During CO_2 Injection and Coalbed Methane Production*, SPE Annual Technical Conference and Exhibition, Denver, Colorado, USA, Sept 21-24, 2008.

(10) Brochard, L.; Vandamme, M.; Pellenq, R. J. M.; Fen-Chong, T. Adsorption-Induced Deformation of Microporous Materials: Coal Swelling Induced by CO_2–CH_4 Competitive Adsorption. *Langmuir* **2011**, *28*, 2659-2670.

(11) White, C. M.; Smith, D. H.; Jones, K. L.; Goodman, A. L.; Jikich, S. A.; LaCount, R. B.; DuBose, S. B.; Ozdemir, E.; Morsi, B. I.; Schroeder, K. T. Sequestration of Carbon Dioxide in Coal with Enhanced Coalbed Methane Recovery a Review†. *Energy Fuels* **2005**, *19*, 659-724.

(12) Harpalani, S.; Prusty, B. K.; Dutta, P. Methane/ CO_2 Sorption Modeling for Coalbed Methane Production and CO_2 Sequestration. *Energy Fuels* **2006**, *20*, 1591-1599.

(13) Khosravi, M.; Bahramian, A.; Emadi, M.; Rostami, B.; Roayaie, E. Mechanistic Investigation of Bypassed-Oil Recovery During CO_2 Injection in Matrix and Fracture. *Fuel* **2014**, *117,* 43-49.

(14) Tudor, R.; Poleschuk, A. Low-Viscosity, Low-Temperature Fracture Fluids. *SPE* **1996**, *35*, 31-36.
(15) Niezgoda, T.; Miedzińska, D.; Małek, E.; Kędzierski, P.; Sławiński, G. Study on Carbon Dioxide Thermodynamic Behavior for the Purpose of Shale Rock Fracturing. *Bull. Pol. Acad. Sci., Tech. Sci.* **2013**, *61*, 605-612.
(16) Ishida, T.; Aoyagi, K.; Niwa, T.; Chen, Y.; Murata, S.; Chen, Q.; Nakayama, Y. Acoustic Emission Monitoring of Hydraulic Fracturing Laboratory Experiment with Supercritical and Liquid CO_2. *Geophys. Res. Lett.* **2012**, *39*, L16309.
(17) Maiti, A. Atomistic Modeling toward High-Efficiency Carbon Capture: A Brief Survey with a Few Illustrative Examples. *Int. J. Greenh. Gas Control* **2014**, *114*, 163-175.
(18) Himeno, S.; Komatsu, T.; Fujita, S. High-Pressure Adsorption Equilibria of Methane and Carbon Dioxide on Several Activated Carbons. *J. Chem. Eng. Data* **2005**, *50*, 369-376.
(19) Huang, L.; Zhang, L.; Shao, Q.; Lu, L.; Lu, X.; Jiang, S.; Shen, W. Simulations of Binary Mixture Adsorption of Carbon Dioxide and Methane in Carbon Nanotubes: Temperature, Pressure, and Pore Size Effects. *J. Phys Chem. C* **2007**, *111*, 11912-11920.
(20) Cavenati, S.; Grande, C. A.; Rodrigues, A. E. Adsorption Equilibrium of Methane, Carbon Dioxide, and Nitrogen on Zeolite 13x at High Pressures. *J. Chem. Eng. Data* **2004**, *49*, 1095-1101.
(21) Bleken, B.-T. L.; Lillerud, K. P.; Splith, T.; Pusch, A.-K.; Stallmach, F. PFG NMR Diffusion Measurements of CH_4 and CO_2 through Large ZSM-58-Crystals. *Microporous Mesoporous Mater.* **2013**, *182*, 25-31.
(22) Ohlin, L.; Bazin, P.; Thibault-Starzyk, F.; Hedlund, J.; Grahn, M. Adsorption of CO_2, CH_4, and H_2O in Zeolite ZSM-5 Studied Using in Situ ATR-FTIR Spectroscopy. *J. Phys Chem. C* **2013**, *117*, 16972-16982.
(23) Wörmeyer, K.; Smirnova, I. Breakthrough Measurements of CO_2 through Aminofunctionalised Aerogel Adsorbent at Low Partial Pressure: Experiment and Modeling. *Microporous Mesoporous Mater.* **2014**, *184*, 61-69.
(24) Mueller, R.; Zhang, S.; Neumann, B.; Bäumer, M.; Vasenkov, S. Self-Diffusion of Carbon Dioxide in Samaria/Alumina Aerogel Catalyst Using High Field NMR Diffusometry. *J. Chem. Phys* **2013**, *139*, 154703.
(25) Golzar, K.; Amjad-Iranagh, S.; Amani, M.; Modarress, H. Molecular Simulation Study of Penetrant Gas Transport Properties into the Pure and Nanosized Silica Particles Filled Polysulfone Membranes. *J. Membr. Sci.* **2014**, *451*, 117-134.
(26) Mebane, D. S.; Kress, J. D.; Storlie, C. B.; Fauth, D. J.; Gray, M. L.; Li, K. Transport, Zwitterions, and the Role of Water for CO_2 Adsorption in Mesoporous Silica-Supported Amine Sorbents. *J. Phys Chem. C* **2013**, *117*, 26617-26627.
(27) Ferey, G.; Serre, C.; Devic, T.; Maurin, G.; Jobic, H.; Llewellyn, P. L.; De Weireld, G.; Vimont, A.; Daturi, M.; Chang, J.-S. Why Hybrid Porous Solids Capture Greenhouse Gases? *Chem. Soc. Rev.* **2011**, *40*, 550-562.
(28) Le, T.; Striolo, A.; Cole, D. R. Propane Simulated in Silica Pores: Adsorption Isotherms, Molecular Structure, and Mobility. *Chem. Eng. Sci.* **2015**, *121*, 292-299.
(29) Gruszkiewicz, M. S.; Rother, G.; Wesolowski, D. J.; Cole, D. R.; Wallacher, D. Direct Measurements of Pore Fluid Density by Vibrating Tube Densimetry. *Langmuir* **2012**, *28*, 5070-5078.
(30) Rother, G.; Melnichenko, Y. B.; Cole, D. R.; Frielinghaus, H.; Wignall, G. D. Microstructural Characterization of Adsorption and Depletion Regimes of Supercritical Fluids in Nanopores†. *J. Phys Chem. C* **2007**, *111*, 15736-15742.
(31) Ho, T. A.; Argyris, D.; Papavassiliou, D. V.; Striolo, A.; Lee, L. L.; Cole, D. R. Interfacial Water on Crystalline Silica: A Comparative Molecular Dynamics Simulation Study. *Mol. Simul.* **2011**, *37*, 172-195.

(32) Rother, G.; Krukowski, E. G.; Wallacher, D.; Grimm, N.; Bodnar, R. J.; Cole, D. R. Pore Size Effects on the Sorption of Supercritical CO_2 in Mesoporous CPG-10 Silica. *J. Phys Chem. C* **2011**, *116*, 917-922.
(33) Arthur, M. A.; Cole, D. R. Unconventional Hydrocarbon Resources: Prospects and Problems. *Elements* **2014**, *10*, 257-264.
(34) Lemmon, E. W.; McLinden, M. O.; Friend, D. G. Thermophysical Properties of Fluid Systems. In *NIST Chemistry WebBook*; NIST Standard Reference Database Number 69; National Institute of Standards and Technology, Gaithersburg MD, 20899, http://webbok.nist.gov, (retrieved July 16, 2013).
(35) Allen, M. P.; Tildesley, D. J. *Computer Simulation of Liquids*; Clarendon Pr.: Oxford, 2004.
(36) Berthelot, D. Sur Le Mélange Des Gaz. *Comptes rendus hebdomadaires des séances de l'Académie des Sciences* **1898**, *126*, 1703-1855.
(37) Lorentz, H. A. Ueber Die Anwendung Des Satzes Vom Virial in Der Kinetischen Theorie Der Gase. *Annalen der Physik* **1881**, *248*, 127-136.
(38) Cygan, R. T.; Liang, J.-J.; Kalinichev, A. G. Molecular Models of Hydroxide, Oxyhydroxide, and Clay Phases and the Development of a General Force Field. *J. Phys Chem. B* **2004**, *108*, 1255-1266.
(39) Martin, M. G.; Siepmann, J. I. Transferable Potentials for Phase Equilibria. 1. United-Atom Description of N-Alkanes. *J. Phys Chem. B* **1998**, *102*, 2569-2577.
(40) Potoff, J. J.; Siepmann, J. I. Vapor–Liquid Equilibria of Mixtures Containing Alkanes, Carbon Dioxide, and Nitrogen. *AIChE Journal* **2001**, *47*, 1676-1682.
(41) Ho, T. A.; Argyris, D.; Cole, D. R.; Striolo, A. Aqueous NaCl and CsCl Solutions Confined in Crystalline Slit-Shaped Silica Nanopores of Varying Degree of Protonation. *Langmuir* **2011**, *28*, 1256-1266.
(42) Babarao, R.; Jiang, J. Diffusion and Separation of CO_2 and CH_4 in Silicalite, C168 Schwarzite, and IRMOF-1: A Comparative Study from Molecular Dynamics Simulation. *Langmuir* **2008**, *24*, 5474-5484.
(43) Hoover, W. G. Canonical Dynamics: Equilibrium Phase-Space Distributions. *Phys. Rev. A* **1985**, *31*, 1695-1697.
(44) Nosé, S. A Molecular Dynamics Method for Simulations in the Canonical Ensemble. *Mol. Phys.* **1984**, *52*, 255-268.
(45) Essmann, U.; Perera, L.; Berkowitz, M. L.; Darden, T.; Lee, H.; Pedersen, L. G. A Smooth Particle Mesh Ewald Method. *J. Chem. Phys* **1995**, *103*, 8577-8593.
(46) Hess, B.; Kutzner, C.; van der Spoel, D.; Lindahl, E. Gromacs 4: Algorithms for Highly Efficient, Load-Balanced, and Scalable Molecular Simulation. *J. Chem. Theory Comput.* **2008**, *4*, 435-447.
(47) Van Der Spoel, D.; Lindahl, E.; Hess, B.; Groenhof, G.; Mark, A. E.; Berendsen, H. J. C. Gromacs: Fast, Flexible, and Free. *J. Comput. Chem.* **2005**, *26*, 1701-1718.
(48) Hockney, R. W.; Goel, S. P.; Eastwood, J. W. Quiet High-Resolution Computer Models of a Plasma. *J. Comput. Phys.* **1974**, *14*, 148-158.
(49) Hirschfelder, J. O.; Curtiss, C. F.; Bird, R. B. *Molecular Theory of Gases and Liquids*; John Wiley & Sons: New York, 1964.
(50) Rother, G.; Vlcek, L.; Gruszkiewicz, M. S.; Chialvo, A. A.; Anovitz, L. M.; Bañuelos, J. L.; Wallacher, D.; Grimm, N.; Cole, D. R. Sorption Phase of Supercritical CO_2 in Silica Aerogel: Experiments and Mesoscale Computer Simulations. *J. Phys Chem. C* **2014**, *118*, 15525-15533.
(51) Argyris, D.; Tummala, N. R.; Striolo, A.; Cole, D. R. Molecular Structure and Dynamics in Thin Water Films at the Silica and Graphite Surfaces. *J. Phys Chem. C* **2008**, *112*, 13587-13599.

(52) Arunan, E.; Desiraju, G. R.; Klein, R. A.; Sadlej, J.; Scheiner, S.; Alkorta, I.; Clary, D. C.; Crabtree, R. H.; Dannenberg, J. J.; Hobza, P., et al. Definition of the Hydrogen Bond (Iupac Recommendations 2011). *Pure Appl. Chem.* **2011**, *83*, 1637-1641.
(53) Sato, H.; Matubayasi, N.; Nakahara, M.; Hirata, F. Which Carbon Oxide Is More Soluble? Ab Initio Study on Carbon Monoxide and Dioxide in Aqueous Solution. *Chem. Phys. Lett.* **2000**, *323*, 257-262.
(54) Kärger, J.; Pfeifer, H. N.M.R. Self-Diffusion Studies in Zeolite Science and Technology. *Zeolites* **1987**, *7*, 90-107.
(55) Sholl, D. S. Testing Predictions of Macroscopic Binary Diffusion Coefficients Using Lattice Models with Site Heterogeneity. *Langmuir* **2006**, *22*, 3707-3714.
(56) Wang, Y.; Mahle, J. J.; Furtado, A. M. B.; Glover, T. G.; Buchanan, J. H.; Peterson, G. W.; LeVan, M. D. Mass Transfer and Adsorption Equilibrium for Low Volatility Alkanes in BPL Activated Carbon. *Langmuir* **2013**, *29*, 2935-2945.
(57) Snurr, R. Q.; Kärger, J. Molecular Simulations and NMR Measurements of Binary Diffusion in Zeolites. *J. Phys Chem. B* **1997**, *101*, 6469-6473.
(58) Vidoni, A. Adsorption and Diffusion of Light Hydrocarbon in DDR Zeolite. Ph.D. Dissertation, The University of Maine, Orono, ME, 2011.
(59) Zhou, J.; Lu, X.; Wang, Y.; Shi, J. Molecular Dynamics Investigation on the Infinite Dilute Diffusion Coefficients of Organic Compounds in Supercritical Carbon Dioxide. *Fluid Phase Equilib.* **2000**, *172*, 279-291.
(60) Feng, H.; Gao, W.; Nie, J.; Wang, J.; Chen, X.; Chen, L.; Liu, X.; Lüdemann, H.-D.; Sun, Z. MD Simulation of Self-Diffusion and Structure in Some N-Alkanes over a Wide Temperature Range at High Pressures. *J. Mol. Model* **2013**, *19*, 73-82.
(61) Elliott, R. W.; Watts, H. Diffusion of Some Hydrocarbons in Air: A Regularity in the Diffusion Coefficients of a Homologous Series. *Can. J. Chem.* **1972**, *50*, 31-34.
(62) Conner, W. C.; Fraissard, J. *Fluid Transport in Nanoporous Materials: Proceedings of the Nato Advanced Study Institute, Held in La Colle Sur Loup, France, 16-28 June 2003*; Springer Netherlands, 2006.
(63) Phan, A.; Ho, T. A.; Cole, D. R.; Striolo, A. Molecular Structure and Dynamics in Thin Water Films at Metal Oxide Surfaces: Magnesium, Aluminum, and Silicon Oxide Surfaces. *J. Phys Chem. C* **2012**, *116*, 15962-15973.

TABLE OF CONTENTS GRAPHIC